Chemically Synthesized Heterostructures of Two-Dimensional Molybdenum/Tungsten-Based Dichalcogenides with Vertically Aligned Layers

Yeonwoong Jung,[†,§] Jie Shen,[†,§] Yong Sun,[‡] and Judy J. Cha[†,§,*]

[†]Department of Mechanical Engineering and Materials Science, Yale University, New Haven, Connecticut 06511, United States, [‡]Micro/Nano Fabrication Laboratory, PRISM, Princeton University, Princeton, New Jersey 08540, United States, and [§]Energy Sciences Institute, Yale University West Campus, West Haven, Connecticut 06477, United States

ABSTRACT We demonstrate a one-step, facile chemical synthesis of heterostructures based on two-dimensional (2D) transition metal dichalcogenides (TMDCs) with vertically aligned 2D layers. Specifically, by using a chemical vapor transport method, we synthesize molybdenum (Mo)/tungsten (W)-based disulfide and diselenide heterostructures, such as MoS_2/WS_2 and $MoSe_2/WSe_2$. Detailed structural characterizations reveal that the 2D layers of two different TMDCs are vertically standing/aligned exposing the edge sites of the layers. The TMDC heterostructure materials exhibit a high uniformity of structural/chemical heterogeneity over a large area (>1 cm^2) and show anisotropic carrier transport properties. These materials with unique heterostructures have great implications for both technological applications and fundamental sciences.

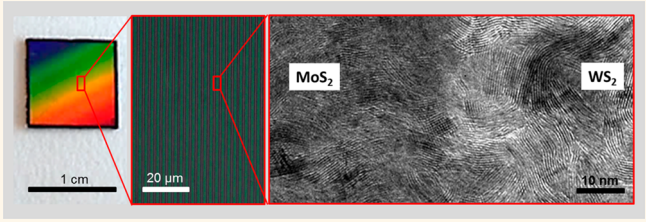

KEYWORDS: chemical synthesis · layered material · two-dimensional crystal · metal dichalcogenide · van der Waals heterostructure · anisotropic transport

Transition metal dichalcogenides (TMDCs) consist of two-dimensional (2D) molecular layers bonded together by weak van der Waals (vdW) attraction owing to their anisotropic bonding nature.[1] Exfoliated 2D layers of TMDCs often present unusual materials properties distinct from their bulk counterparts, thus offering opportunities for technological applications. For example, molybdenum (Mo) and tungsten (W)-based derivatives present tunable bandgap energies matching the solar spectrum and indirect-to-direct bandgap transition,[1−3] making them promising for optoelectronic applications. Recently, substantial efforts have been made in the heterogeneous integration of multiple 2D TMDC layers with distinct materials properties to realize unprecedented functionalities.[4] First principle calculations of heterostructure Mo/W−disulfides (also, diselenides) (MoS_2/WS_2 and $MoSe_2/WSe_2$) suggest tunable/direct bandgap energies distinct from their individual counterparts,[5,6] and energy band alignment suitable for water splitting and photovoltaics.[7] Experimentally, strong light-matter interactions and rectifying electronic junctions have been demonstrated in MoS_2/graphene, MoS_2/carbon nanotube, and WS_2/graphene,[8−10] as well as MoS_2/WSe_2 systems.[11−13] The realization of such heterostructures has so far relied on the mechanical assembly of exfoliated individual 2D layers utilizing their intermolecular vdW attraction. This manual integration method is, however, inefficient and potentially not suitable for the high-yield/scaled-up production of materials for practical applications. More reliable integration methods should be pursued in the context of chemical synthesis approaches, such as chemical vapor deposition techniques. A few works have been demonstrated for the chemical synthesis of graphene-based heterostructure systems.[14,15] Yet, large-area/controlled synthesis of heterostructures solely

* Address correspondence to judy.cha@yale.edu.

Received for review July 14, 2014 and accepted August 25, 2014.

Published online August 25, 2014
10.1021/nn503853a

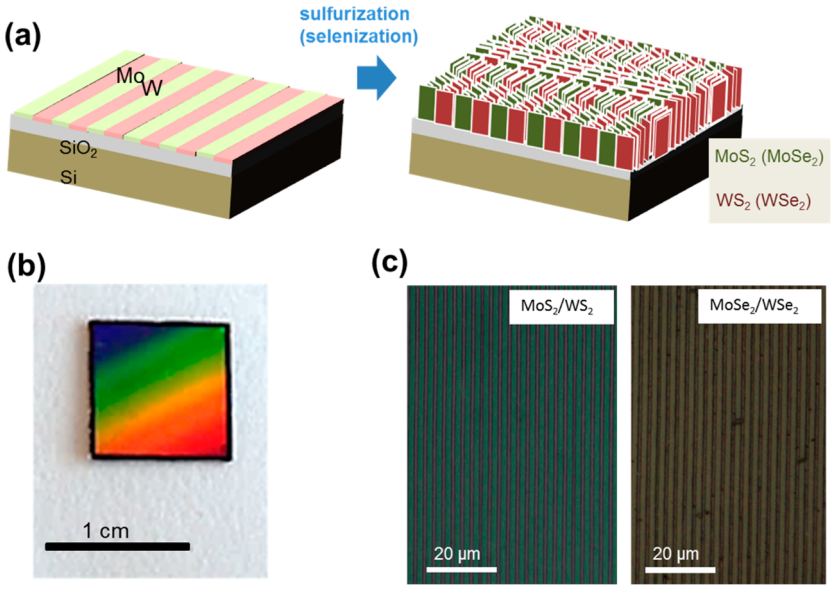

Figure 1. Synthesis of TMDC heterostructure films with vertically aligned 2D layers. (a) Schematic to depict the synthesis process of TMDC heterostructure films with vertically aligned 2D layers. (b) Photography image of a MoS_2/WS_2 heterostructure film grown on a SiO_2/Si substrate. (c) Zoomed-in optical microscopy images of MoS_2/WS_2 (left) and $MoSe_2/WSe_2$ (right) heterostructure films.

based on multiple 2D TMDCs has remained unexplored. Besides potential technological applications, 2D TMDC heterostructure systems are also important from a fundamental science point of view. As the individual building blocks of vdW heterostructures approach a molecular level, carrier transport is likely dominated by the interfacial properties of adjacent 2D layers with lattice mismatch. Therefore, precise control/characterizations of 2D vdW interfaces and the study of their effect on transport properties are essential. Despite the scientific significance, such studies have been largely unexplored so far. This is mainly due to the lack of appropriate TMDC heterostructure systems where the structural orientation of individual 2D layers is highly controlled to allow the direct characterizations of 2D vdW interfaces.

Recently, a new class of TMDCs has been developed where the 2D molecular layers are vertically assembled to preferably expose the edge-sites of the layers rather than basal planes.[16−18] These TMDCs with vertically aligned 2D layers present unique materials platforms for both technological applications and fundamental scientific studies. Owing to the enhanced chemical reactivity of the preferably exposed dangling bonds on the edge sites, they are useful for catalytic-reaction based electrochemical applications such as hydrogen-evolution-reaction (HER).[16,17] These TMDCs also make an ideal model system which offers unique advantages for the aforementioned interfacial studies. Benefiting from the vertical orientation of 2D layers, an atomic-level, top-to-down characterization of the vdW interfaces is possible with transmission electron microscopy (TEM). Simultaneously, tuning the 2D vdW interfaces can be carried out by physical/chemical methods (*e.g.*, heating, intercalations), and their correlation with transport properties can be investigated in an *in situ* manner in TEM. In this regard, chemically synthesized TMDC heterostructures based on vertically aligned 2D layers combine the technological potential of heterostructures and the scientific opportunities for the study of 2D vdW interface properties.

Herein, we demonstrate one-step, facile chemical synthesis of 2D TMDC heterostructure films with well-defined structures and compositions over a large area. Specifically, by using a chemical vapor-deposition method, we synthesize two classes of 2D TMDC heterostructures: MoS_2/WS_2 and $MoSe_2/WSe_2$ with vertically aligned 2D layers covering over an area of >1 cm^2.

RESULTS AND DISCUSSION

Figure 1a illustrates the growth scheme for MoS_2/WS_2 ($MoSe_2/WSe_2$) heterostructure films with vertically aligned 2D layers. Mo/W thin films with periodic line patterns (thickness 10−20 nm, line width 1−2 μm) are prepared on SiO_2/Si substrates, which function as growth substrates. The patterned substrates are then rapidly sulfurized (selenized) by evaporating elemental sulfur (selenium) inside a growth furnace, which lead to the growth of MoS_2/WS_2 ($MoSe_2/WSe_2$) heterostructure films with vertically aligned 2D layers. Refer to the Methods section for growth details and substrates preparation. Figure 1b shows a representative optical microscopy image of a large-area heterostructure film grown on a SiO_2/Si substrate (MoS_2/WS_2 in this case). The color dispersion indicates the high periodicity (1 μm line-width) of the grown materials over the entire growth substrate (1 cm × 1 cm). Figure 1c shows close-up view images of MoS_2/WS_2 (left) and

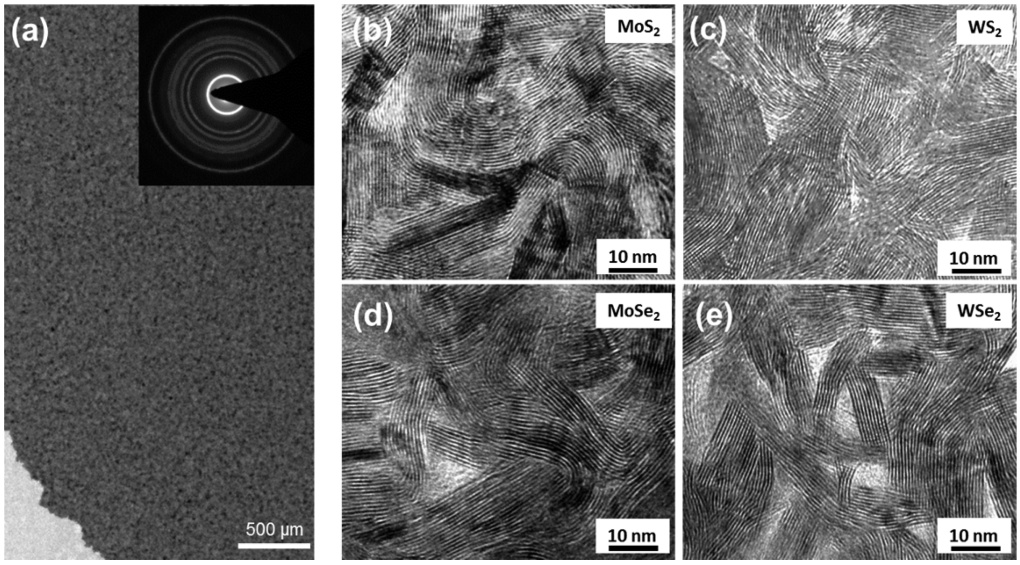

Figure 2. TEM characterizations of TMDC films with vertically aligned 2D layers. (a) TEM image of a large-area $MoSe_2$ film with its corresponding SAED pattern (inset). (b−e) HRTEM images of (b) MoS_2, (c) WS_2, (d) $MoSe_2$, and (e) WSe_2 films with vertically aligned 2D layers.

$MoSe_2$/WSe_2 (right) heterostructure films. After the growth, the thickness of the initial metal layers changes dramatically. For example, initially ~10 nm thick Mo and W seed layers turned to ~35 nm thick MoS_2 and WS_2 films.

MoS_2/WS_2 ($MoSe_2$/WSe_2) heterostructure films are further characterized in detail. For comparison, we first grew reference samples of individual MoS_2, WS_2, $MoSe_2$ and WSe_2 with vertically aligned 2D layers and characterized their morphology. Growths for these individual TMDCs were performed under the identical growth conditions used for the heterogrowth (see Methods section for growth details). Figure 2a shows a representative TEM image of a large-area TMDC film with vertically aligned 2D layers ($MoSe_2$ in this case). The inset shows a selective area electron diffraction (SAED) pattern of the corresponding film, revealing its polycrystalline structure. Figure 2b−e shows the high-resolution TEM (HRTEM) images of MoS_2, WS_2, $MoSe_2$, and WSe_2 films with vertically aligned 2D layers, respectively. The images clearly reveal highly dense, all vertically aligned 2D layers with exposed edge sites in all these films. Such morphology has been consistently observed in all TEM samples collected from arbitrary areas of the growth substrates (>1 cm x 1 cm), confirming the large-scale/high-yield of the vertical growth. The spacing between adjacent 2D layers is determined from HRTEM images as well as high angle annular dark field (HAADF) scanning TEM (STEM). The interlayer spacing is measured to be ~0.63 nm for both MoS_2 and WS_2 (Supporting Information, Figure S1), which corresponds to the hexagonal (002) crystalline plane and is consistent with previous studies.[18−20]

We, then, characterized the morphology of the TMDC heterostructure films with TEM. Figure 3 shows

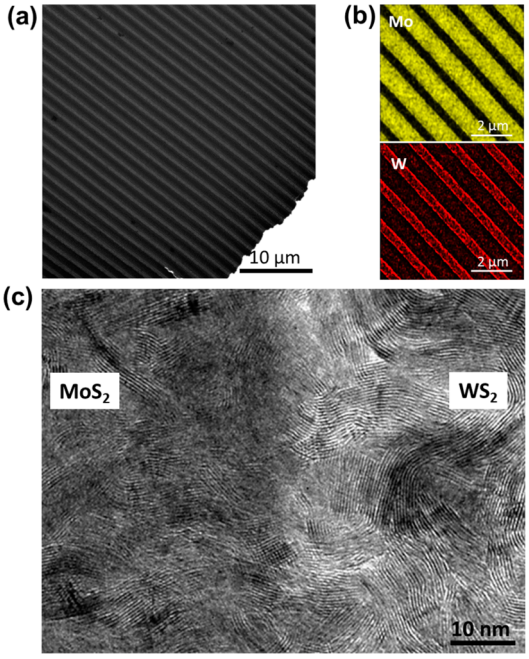

Figure 3. TEM characterizations of 2D TMDC heterostructure films with vertically aligned 2D layers. (a) Low-magnification bright-field TEM image of a MoS_2/WS_2 heterostructure film with vertically aligned 2D layers. (b) STEM-EDS elemental mapping images to show the spatial distribution of Mo and W. (c) HRTEM image of a MoS_2/WS_2 interface with vertically aligned 2D layers.

detailed TEM characterizations of a MoS_2/WS_2 film. A bright-field low-magnification TEM image (Figure 3a) shows a MoS_2/WS_2 film lifted off from a growth substrate and transferred to a carbon-coated TEM grid. The periodic imaging contrast difference over a large-area suggests the heterogeneity of the film. STEM energy dispersive X-ray spectroscopy (EDS) elemental mapping images (Figure 3b) show the spatial distribution of

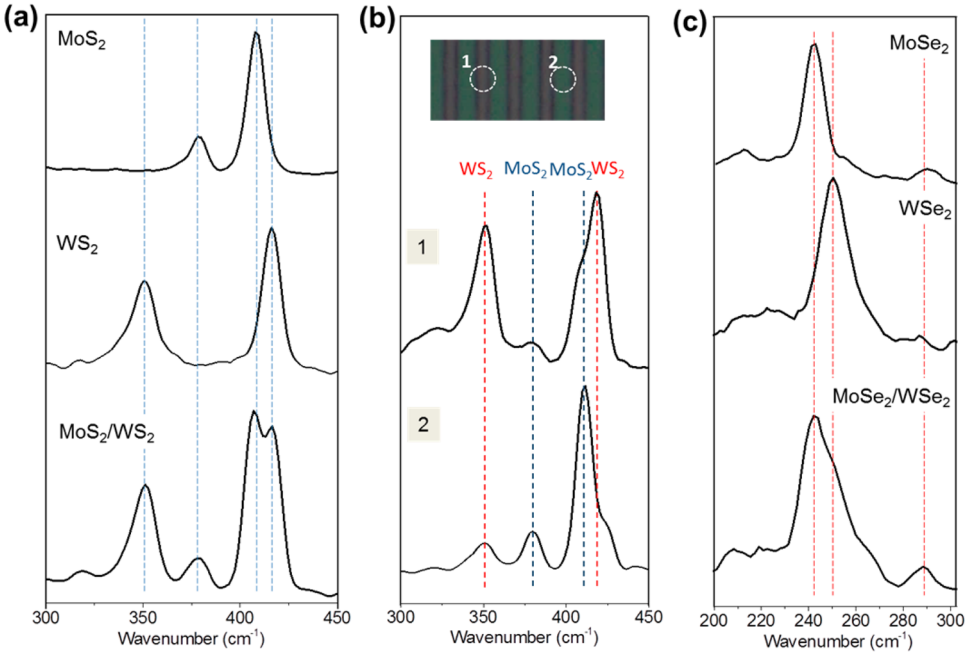

Figure 4. Raman characterizations of individual and heterostructure TMDC films with vertically aligned 2D layers. (a) Comparison of the Raman spectra from MoS_2, WS_2, and MoS_2/WS_2 heterostructure films with vertically aligned 2D layers. (b) Site-specific Raman spectra from a MoS_2/WS_2 heterostructure film with vertically aligned 2D layers; WS_2-dominat, and MoS_2-dominant Raman spectra are collected from the region of (1) and (2) in the top image, respectively. (c) Comparison of the Raman spectra from $MoSe_2$, WSe_2, and $MoSe_2/WSe_2$ heterostructure films with vertically aligned 2D layers.

Mo and W in the film, revealing their periodic distribution. Remarkably, the HRTEM image (Figure 3c) across the interface of a MoS_2/WS_2 pattern shows the continuation of vertically aligned 2D layers. Identifying the exact physical interface is difficult as some vertically aligned 2D layers are grown to overlap with each other at the interface.

The morphologies of the individual TMDC films and heterostructure films with vertically aligned 2D layers were further characterized and compared by Raman spectroscopy (532 nm wavelength, beam diameter ~20 μm). Figure 4a compares the Raman spectra of individual MoS_2 and WS_2 films with vertically aligned 2D layers, and a MoS_2/WS_2 heterostructure film. The Raman peak positions of the MoS_2/WS_2 film are the summation of those of individual films (MoS_2, ~383 cm^{-1} for E^1_{2g} and ~408 cm^{-1} for A_{1g}; WS_2 ~352 cm^{-1} for E^1_{2g} and ~418 cm^{-1} for A_{1g}[18,21]) without any indication for the formation of $Mo_xW_{1-x}S$ alloy. In alloyed $Mo_xW_{1-x}S$ in the literature,[22,23] Raman peaks are shifted toward each characteristic peaks of MoS_2 and WS_2, which we do not observe. The spatial distribution of each MoS_2 and WS_2 was further confirmed by focusing the Raman laser beam (Figure 4b). When a confined Raman laser beam (diameter ~1.5 μm with a filter) is focused on the separate regions of the MoS_2/WS_2 film ((1) and (2) in Figure 4b top), distinct WS_2- and MoS_2-dominant Raman spectra appear from each region. The presence of the weak MoS_2 (WS_2) Raman signals from the WS_2 (MoS_2)-dominant regions is due to the laser beam spot being slightly larger than the line-width (1 μm) of the pattern. This Raman characterization confirms the chemical and structural heterogeneity of the grown materials, which is predetermined by the spatial location of the initial Mo/W patterns. $MoSe_2/WSe_2$ heterostructure films also present distinct Raman characteristics of each $MoSe_2$ and WSe_2 with vertically aligned 2D layers (Figure 4c) ($MoSe_2$, ~289 cm^{-1} for E^1_{2g} and ~242 cm^{-1} for A_{1g}; WS_2, ~252 cm^{-1} for both E^1_{2g} and A_{1g}[18,21]). One typical Raman characteristics of these 2D TMDCs films with vertically aligned 2D layers is that the intensity of A_{1g} (out-of-plane vibration mode) is much higher than E^1_{2g} (in-plane vibration mode). This is a clear indication of the dominant vertical orientation of individual layers (dominant out-of-plane vibration exposing edge sites), consistent with previous studies.[18,21,24] For example, mono-to-a-few-layer horizontally grown 2D WS_2 present much smaller intensity of A_{1g} peak over other peaks under the same 532 nm laser excitation,[25] different from the characteristics observed in the films with vertically aligned 2D layers. These Raman and TEM characterizations confirm that two different TMDC materials with vertically aligned 2D layers are grown maintaining their structural/chemical heterogeneity over a large area.

We note that the growth of TMDC heterostructure films was realized on SiO_2/Si substrates which are compatible with various microelectronic processes adopted for the patterning of initial Mo and W (*e.g.*, optical lithography and reactive ion etching (RIE)). These complicated processes coupled with high

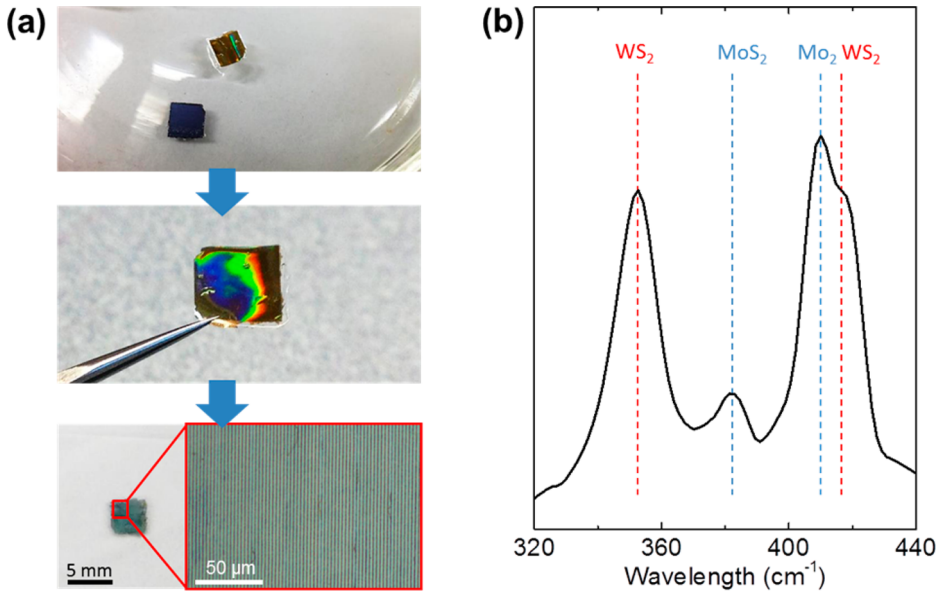

Figure 5. Transfer of large-area TMDC heterostructure films. (a) Demonstration of the transfer of a large-area MoS_2/WS_2 heterostructure film with vertically aligned 2D layers. (b) Raman characterizations of a MoS_2/WS_2 heterostructure film transferred onto a glass slide.

growth temperature make the direct patterning/growth of the heterostructure films on various substrates difficult, thus potentially limit their versatilities and functionalities. By using a simple, polymer-based transfer method, we demonstrate that large-area TMDC heterostructure films with vertically aligned 2D layers can be transferred onto arbitrary substrates maintaining their structural integrity. The transfer method is similar to those previously reported.[26] Figure 5a illustrates the steps for the transfer of TMDC heterostructure films. As-grown TMDC MoS_2/WS_2 heterostructure films on SiO_2/Si substrates were first deposited with poly(methyl methacrylate) (PMMA) followed by curing. The substrates were subsequently immersed in potassium hydroxide (KOH) solution at 80 °C for a selective etching of SiO_2. A photography image of a large-area PMMA/MoS_2/WS_2 heterostructure film shows that it is lifted off the growth substrate floating on the KOH solution (Figure 5a top). Unlike the mono-to-a-few-layer TMDCs which are difficult to handle with a tweezer, these PMMA/TMDC heterostructure films can be easily picked up by a tweezer (Figure 5a mid). This is because the film has a large thickness (>50 nm for initial 20 nm seed metals) due to the vertically preferred growth orientation of 2D layers. The lifted PMMA/heterostructure film presents a clear color dispersion reflecting the high periodicity of the grown materials. The PMMA/TMDC film can be transferred onto arbitrary substrates followed by the dissolution of PMMA with acetone. A photography image of the same film transferred onto a glass slide is presented (Figure 5a bottom). A slight loss of the film occurred at its edge during the complete removal of the PMMA with acetone. Nevertheless, a majority of the film remains intact as reflected by the highly periodic pattern of MoS_2 and WS_2 (Figure 5a, bottom inset). The morphology of the heterostructure film after transfer was characterized by Raman spectroscopy. Figure 5b shows the Raman spectrum from the same MoS_2/WS_2 heterostructure film transferred on the glass slide, revealing characteristics similar to those of as-grown films on SiO_2/Si substrates in Figure 4a. The results confirm that large-area TMDC heterostructure films with vertically aligned 2D layers can be transferred to arbitrary substrates maintaining their structural integrity during the lift-off/transfer process.

The structural/chemical heterogeneity of TMDC heterostructure films with vertically aligned 2D layers is reflected on their physical properties. We investigated the carrier transport properties of these films by measuring their two-terminal current (I)−voltage (V) characteristics. Electrical characterizations were performed with two different metal electrodes configurations: perpendicular and parallel to the orientation of the TMDC line patterns. Figure 6a,b compares the $I-V$ characteristics of a $MoSe_2/WSe_2$ heterostructure film with perpendicular (Figure 6a, inset) and parallel (Figure 6b) contacts. The length between electrodes is 16 μm, covering 4 $MoSe_2$ and 4 WSe_2 line patterns (line width 2 μm). Highly linear $I-V$ is observed with the perpendicular contact (Figure 6a), while rectifying $I-V$ is observed with the parallel contact (Figure 6b). This anisotropy reflects that the spatially controlled chemical heterogeneity of the heterostructure film presents distinct carrier transport properties. To better understand this, we characterized the carrier transport properties of individual $MoSe_2$ and WSe_2 films. Field-effect-transistors (FETs) were fabricated by transferring each

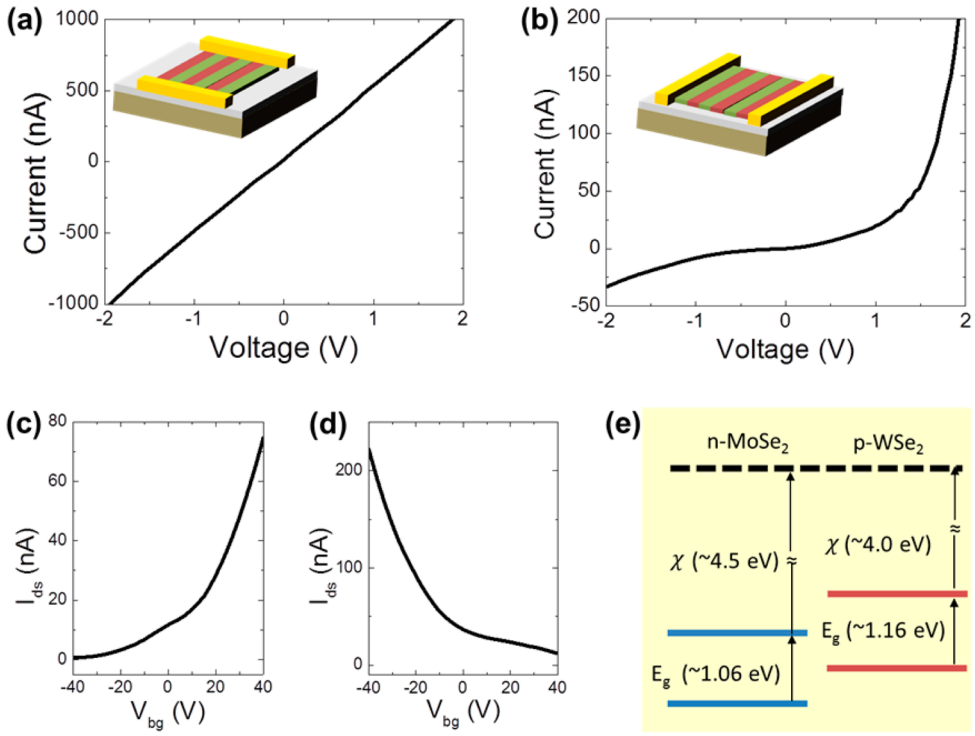

Figure 6. Electrical characterizations of TMDC heterostructure films. (a and b) Two-terminal *I*−*V* characterizations of a $MoSe_2$/WSe_2 heterostructure film with (a) perpendicular electrodes,and (b) parallel electrodes. (c and d) FET characterizations of (c) $MoSe_2$ and (d) WSe_2 FETs, showing n-type and p-type gate responses, respectively. (f) Ideal band diagram for p-WSe_2/n-$MoSe_2$ with bulk properties showing type II heterojunction.

$MoSe_2$ and WSe_2 film onto heavily doped SiO_2/Si substrates following the transfer method in Figure 5. Characteristics of source-drain current (I_{ds}) *vs* back gate voltage (V_{bg}) are characterized for $MoSe_2$ (Figure 6c) and WSe_2 (Figure 6d) FETs. The $MoSe_2$ and WSe_2 FETs present n-type and p-type characteristics under back-gate biasing (constant bias, V_{ds} = 15 V), respectively. The results are consistent with the carrier types of chemically synthesized polycrystalline $MoSe_2$[27−29] and WSe_2[27,30,31] in the literature. This suggests that the observed rectifying *I*−*V* is attributed to the p−n junctions at the interfaces of p-WSe_2/n-$MoSe_2$. Control experiments of two-terminal *I*−*V* characterizations on WSe_2 and $MoSe_2$ films show Ohmic transport for both, consistent with Figure 6a. Therefore, we rule out the possibility that the observed rectification might be originating from a Schottky junction at one end of the electrodes. Indeed, highly rectifying *I*−*V* with a diode ideality factor ~2 was previously reported in bulk p-WSe_2/n-$MoSe_2$,[27] which is consistent with our observation. On the basis of the bulk materials parameters for WSe_2 and $MoSe_2$ (*e.g.*, bandgap energy (E_g) of ~1.06 eV for $MoSe_2$ and ~1.16 eV for WSe_2, electron affinity (χ) of ~4.5 eV for $MoSe_2$ and ~4.0 eV for WS_2) known in the literature,[27,32] an ideal band diagram is constructed for a p-WSe_2/n-$MoSe_2$ interface (Figure 6e). The diagram reveals a type II heterojunction of p-WSe_2/n-$MoSe_2$ indicating a formation of a built-in potential which leads to rectifying *I*−*V*, as also previously suggested.[27] Similar anisotropic carrier transport is also observed for MoS_2/WS_2 heterostructure films (Supporting Information, Figure S2). The current rectification ratio (<50 at ±1 V) of our TMDC heterostructure films is smaller than those of other mechanically exfoliated/stacked 2D heterostructure systems (*e.g.*, WSe_2/graphene,[8] MoS_2/graphene (or, carbon nanotube),[9,10] and MoS_2/WSe_2[11,12]). This is possibly due to that the mechanically exfoliated/stacked 2D heterostructures possess atomically sharp, abrupt junctions,[12] while the interfaces of our chemically synthesized TMDC heterostructure films are diffusive as shown in Figure 3c. In addition, the carrier transport in the TMDC films with vertically aligned 2D layers is dominated by a cross-plane hopping mechanism[33,34] (opposed to the in-plane transport in horizontal 2D films), as indicated by their small FET mobilities (typically, ≤0.01 cm^2/V s); the FET mobility μ is extracted from the linear regime of the transport plots (Figure 6c,d) using the equation $\mu = [dI_{ds}/dV_{bg}] \times [L/(WC_{ox}V_{ds})]$, where *L*, *W*, and C_{ox} are the channel length, width, and the gate capacitance per unit area.[35] This analysis suggests that the transport properties of our TMDC heterostructure films are limited at present, thus, much work is needed to improve them. For example, the synthesis of heterostructure films with vertically and laterally aligned layers would present well-defined hetero-vdW interfaces, which is currently under investigation.

Despite the presently limited carrier transport properties, we believe that these novel 2D TMDC

heterostructures with vertically aligned 2D layers are intriguing building blocks for a variety of potential applications and fundamental science. For example, the chemically active edge sites inherent to the vertically exposed layers are promising for catalytic applications as previously demonstrated,[17,18,21] while the spatial control of chemical compositions may provide additional functionalities such as site-specific catalytic activities. In addition, the dominant out-of-plane carrier transport properties combined with periodically tunable chemical compositions can be useful for thermoelectric applications. Indeed, WSe_2 thin films with horizontally stacked basal planes present the lowest room-temperature thermal conductivity ever observed in fully dense solids, owing to the suppressed in-plane thermal transport.[36] The combined features of chemical composition control and vertically aligned basal planes of 2D TMDC heterostructure films may present an opportunity to design novel superlattice thermoelectric materials.[37] We emphasize that our synthesis method can be generalized to other TMDCs beyond the Mo- and W-based ones owing to the chemical-composition controllability of seed metals.

CONCLUSION

In summary, we demonstrate a one-step, facile synthesis of MoS_2/WS_2 and $MoSe_2/WSe_2$ heterostructure films with vertically aligned 2D layers. Detailed structural characterizations reveal that these heterostructure TMDCs possess vertically aligned 2D layers of two different TMDCs over a large area (>1 cm^2). This structural/chemical heterogeneity is also manifested by highly anisotropic carrier transport properties. We further demonstrate a facile transfer of these heterostructure TMDCs onto arbitrary substrates, which broaden the utility of these materials. These uniquely structured TMDC heterostructures possess a great potential for a variety of technological applications as well as fundamental scientific studies.

METHODS

Materials Growth and Substrates Preparation. TMDC heterostructure films with vertically aligned 2D layers are grown inside a single-zone horizontal tube furnace (Lindberg/Blue M). Mo/W thin film-deposited SiO_2/Si substrates are used as growth substrates, which are lithographically patterned in the following procedure. W thin film is first sputtered on a SiO_2/Si substrate followed by the spin-coating of bilayer photoresists (AZ1505 and LOR3A). The substrate is exposed under a patterned photomask with a 405 nm laser writer (Heidelberg DWL66) and developed (AZ300MIF). The patterned W film is, then, selectively etched in a reactive-ion-etcher (Plasma-Therm 790). Mo is subsequently sputtered onto the W-etched areas followed by a lift-off (Microposit remover 1165), which results in the final pattern of Mo/W lines. The patterned Mo/W substrates are placed in the central zone of the growth furnace, and elemental sulfur (selenium) powders (Sigma-Aldrich) are placed at the upstream side of the furnace for the growth of heterostructure films. The tube furnace is pumped down to a base pressure of ~5 mTorr and flushed with Ar gas to remove residual oxygen inside the tube. Subsequently, the furnace is heated to the growth temperature (~700−800 °C) with a total ramping time of ~20 min and is maintained for 15 min followed by a natural cooling. During the reaction (including the cooling stage), the furnace is saturated with vaporized sulfur (selenium) under Ar atmosphere (flow rate; 150 standard cubic centimeters per minute (SCCM)). The vapor pressure throughout the entire reaction is maintained to be ~350 mTorr.

Morphological/Electrical Characterizations. The morphology of TMDC films with vertically aligned 2D layers is characterized using TEM/STEM (FEI Tecnai Osiris 200 kV) and Raman spectroscopy (Horiba-Jobin Yvon HR-800 equipped with a green laser tuned to 532 nm). For TEM sample preparation, droplets of buffered oxide etchant (BOE: 1:10 volume ratio of 40%NH_4F in water to 49% HF in water) are applied to as-grown TMDC films on SiO_2/Si substrates, which etches the SiO_2 layer. The TMDC films dispersed in the BOE are subsequently transferred to carbon-coated copper TEM grids. For the FET and two-terminal electrical characterizations of individual TMDC and heterostructure films, as-grown films were transferred to back-side metallized heavily doped SiO_2/Si substrates using the method in Figure 5. Gold (Au) electrodes are patterned on top of the films using a shadow mask, which defines FET channel and electrodes dimensions. All the electrical characterizations are carried out with HP 4545 device parameter analyzer.

Conflict of Interest: The authors declare no competing financial interest.

Supporting Information Available: HAADF characterizations of MoS_2 and WS_2 with vertically aligned 2D layers and anisotropic carrier transport for MoS_2/WS_2 heterostructure film. This material is available free of charge *via* the Internet at http://pubs.acs.org.

Acknowledgment. Microscopy facilities used in this work were supported by the Yale Institute for Nanoscience and Quantum Engineering and National Science Foundation MRSEC DMR 1119826. The authors also acknowledge the use of facilities of the Micro/Nanofabrication Laboratory (MNFL) at the Princeton Institute for the Science and Technology of Materials (PRISM).

REFERENCES AND NOTES

1. Wang, Q. H.; Kalantar-Zadeh, K.; Kis, A.; Coleman, J. N.; Strano, M. S. Electronics and Optoelectronics of Two-Dimensional Transition Metal Dichalcogenides. *Nat. Nanotechnol.* **2012**, *7*, 699–712.
2. Mak, K. F.; Lee, C.; Hone, J.; Shan, J.; Heinz, T. F. Atomically Thin MoS_2: A New Direct-Gap Semiconductor. *Phys. Rev. Lett.* **2010**, *105*, 136805.
3. Splendiani, A.; Sun, L.; Zhang, Y.; Li, T.; Kim, J.; Chim, C.-Y.; Galli, G.; Wang, F. Emerging Photoluminescence in Monolayer MoS_2. *Nano Lett.* **2010**, *10*, 1271–1275.
4. Geim, A. K.; Grigorieva, I. V. Van der Waals Heterostructures. *Nature* **2013**, *499*, 419–425.
5. Terrones, H.; López-Urías, F.; Terrones, M. Novel Hetero-Layered Materials with Tunable Direct Band Gaps by Sandwiching Different Metal Disulfides and Diselenides. *Sci. Rep.* **2013**, *3*, 1549.
6. Kosmider, K.; Fernández-Rossier, J. Electronic Properties of the MoS_2-WS_2 Heterojunction. *Phys. Rev. B* **2013**, *87*, 075451.
7. Kang, J.; Tongay, S.; Zhou, J.; Li, J.; Wu, J. Band Offsets and Heterostructures of Two-Dimensional Semiconductors. *Appl. Phys. Lett.* **2013**, *102*, 012111.
8. Britnell, L.; Ribeiro, R. M.; Eckmann, A.; Jalil, R.; Belle, B. D.; Mishchenko, A.; Kim, Y.-J.; Gorbachev, R. V.; Georgiou, T.; Morozov, S. V.; *et al.* Strong Light-Matter Interactions in Heterostructures of Atomically Thin Films. *Science* **2013**, *340*, 1311–1314.

9. Jariwala, D.; Sangwan, V. K.; Wu, C.-C.; Prabhumirashi, P. L.; Geier, M. L.; Marks, T. J.; Lauhon, L. J.; Hersam, M. C. Gate-Tunable Carbon Nanotube−MoS_2 Heterojunction p-n Diode. *Proc. Natl. Acad. Sci. U.S.A.* **2013**, *110*, 18076–18080.
10. Yu, W. J.; Liu, Y.; Zhou, H.; Yin, A.; Li, Z.; Huang, Y.; Duan, X. Highly Efficient Gate-Tunable Photocurrent Generation in Vertical Heterostructures of Layered Materials. *Nat. Nanotechnol.* **2013**, *8*, 952–958.
11. Furchi, M. M.; Pospischil, A.; Libisch, F.; Burgdörfer, J.; Mueller, T. Photovoltaic Effect in an Electrically Tunable van der Waals Heterojunction. *Nano Lett.* **2014**, *14*, 4785–4791.
12. Cheng, R.; Li, D.; Zhou, H.; Wang, C.; Yin, A.; Jiang, S.; Liu, Y.; Chen, Y.; Huang, Y.; Duan, X. Electroluminescence and Photocurrent Generation from Atomically Sharp WSe_2/MoS_2 Heterojunction p-n Diodes. **2014** , arXiv:1403.3447. arXiv.org e-Print archive. http://arxiv.org/abs/1403.3447.
13. Lee, C.-H.; Lee, G.-H.; van der Zande, A. M.; Chen, W.; Li, Y.; Han, M.; Cui, X.; Arefe, G.; Nuckolls, C.; Heinz, T. F.; *et al.* Atomically Thin p-n Junctions with van der Waals Heterointerfaces. **2014**, arXiv:1403.3062. arXiv.org e-Print archive. http://arxiv.org/abs/1403.3062
14. Liu, L.; Park, J.; Siegel, D. A.; McCarty, K. F.; Clark, K. W.; Deng, W.; Basile, L.; Idrobo, J. C.; Li, A.-P.; Gu, G. Heteroepitaxial Growth of Two-Dimensional Hexagonal Boron Nitride Templated by Graphene Edges. *Science* **2014**, *343*, 163–167.
15. Tang, S.; Wang, H.; Zhang, Y.; Li, A.; Xie, H.; Liu, X.; Liu, L.; Li, T.; Huang, F.; Xie, X.; Jiang, M. Precisely Aligned Graphene Grown on Hexagonal Boron Nitride by Catalyst Free Chemical Vapor Deposition. *Sci. Rep.* **2013**, *3*, 2666.
16. Kibsgaard, J.; Chen, Z.; Reinecke, B. N.; Jaramillo, T. F. Engineering the Surface Structure of MoS_2 to Preferentially Expose Active Edge Sites for Electrocatalysis. *Nat. Mater.* **2012**, *11*, 963–969.
17. Wang, H.; Lu, Z.; Xu, S.; Kong, D.; Cha, J. J.; Zheng, G.; Hsu, P.-S.; Yan, K.; Bradshaw, D.; Prinz, F. B.; Cui, Y. Electrochemical Tuning of Vertically Aligned MoS_2 Nanofilms and Its Application in Improving Hydrogen Evolution Reaction. *Proc. Natl. Acad. Sci. U.S.A.* **2013**, *110*, 19701–19706.
18. Kong, D.; Wang, H.; Cha, J. J.; Pasta, M.; Koski, K. J.; Yao, J.; Cui, Y. Synthesis of MoS_2 and $MoSe_2$ Films with Vertically Aligned Layers. *Nano Lett.* **2013**, *13*, 1341–1347.
19. Liu, H.; Su, D.; Wang, G.; Qiao, S. Z. An Ordered Mesoporous WS_2 Anode Material with Superior Electrochemical Performance for Lithium Ion Batteries. *J. Mater. Chem.* **2012**, *22*, 17437–17440.
20. Yang, H.; Liu, S.; Li, J.; Li, M.; Peng, G.; Zou, G. Synthesis of Inorganic Fullerene-likeWS_2 Nanoparticles and Their Lubricating Performance. *Nanotechnology* **2006**, *17*, 1512–1519.
21. Wang, H.; Kong, D.; Johanes, P.; Cha, J. J.; Zheng, G.; Yan, K.; Liu, N.; Cui, Y. $MoSe_2$ and WSe_2 Nanofilms with Vertically Aligned Molecular Layers on Curved and Rough Surfaces. *Nano Lett.* **2013**, *13*, 3426–3433.
22. Chen, Y.; Xi, J.; Dumcenco, D. O.; Liu, Z.; Suenaga, K.; Wang, D.; Shuai, Z.; Huang, Y.-S.; Xie, L. Tunable Band Gap Photoluminescence from Atomically Thin Transition-Metal Dichalcogenide Alloys. *ACS Nano* **2013**, *7*, 4610–4616.
23. Dumcenco, D. O.; Chen, K. Y.; Wang, Y. P.; Huang, Y. S.; Tiong, K. K. Raman Study of 2H-$Mo_{1-x}W_xS_2$ Layered Mixed Crystals. *J. Alloys. Compd.* **2010**, *506*, 940–943.
24. Gaur, A. P. S.; Sahoo, S.; Ahmadi, M.; Guinel, M. J.-F.; Gupta, S. K.; Pandey, R.; Dey, S. K.; Katiyar, R. S. Optical and Vibrational Studies of Partially Edge-Terminated Vertically Aligned Nanocrystalline MoS_2 Thin Films. *J. Phys. Chem. C* **2013**, *117*, 26262–26268.
25. Zhao, W.; Ghorannevis, Z.; Kumar, A. K.; Pang, J. R.; Toh, M.; Zhang, X.; Kloc, C.; Tane, P. H.; Eda, G. Lattice Dynamics in Mono- and Few-Layer Sheets of WS_2 and WSe_2. *Nanoscale* **2013**, *5*, 9677–9683.
26. van der Zande, A. M.; Huang, P. Y.; Chenet, D. A.; Berkelbach, T. C.; You, Y.; Lee, G.-H.; Heinz, T. F.; Reichman, D. R.; Muller, D. A.; Hone, J. C. Grains and Grain Boundaries in Highly Crystalline Monolayer Molybdenum Disulphide. *Nat. Mater.* **2013**, *12*, 554.
27. Späh, R.; Lux-Stenier, M.; Obergfell, M.; Bucher, E.; Wagner, S. n-$MoSe_2$/p-WSe_2 Heterojunctions. *Appl. Phys. Lett.* **1985**, *47*, 871–873.
28. Ang, P. G. P.; Sammells, A. F. n-$MoSe_2$ Photoelectrochemical Halogen Storage Cell. *J. Electrochem. Soc.* **1982**, *129*, 233–235.
29. El-Mahalawy, S. H.; Evans, B. L. The Thermal Expansion of 2H-MoS_2, 2H-$MoSe_2$ and 2H-WSe_2 between 20 and 800°C. *J. Appl. Crystallogr.* **1976**, *9*, 403–406.
30. Jäger-Waldau, A.; Bucher, E. WSe_2 Thin Films Prepared by Soft Selenization. *Thin Solid Films* **1991**, *200*, 157–164.
31. Agarwal, M. K.; Rao, V. V.; Pathak, V. M. Growth of n-type and p-type WSe_2 Crystals Using $SeCl_4$ Transporter and their Characterization. *J. Cryst. Growth.* **1989**, *97*, 675–679.
32. Novel Materials Development NREL/SR-520-44020 for Polycrystalline Thin-Film November 2008 Solar Cells, http://www.nrel.gov/docs/fy09osti/44020.pdf.
33. Tang, H.; Morrison, S. R. Optimization of the Anisotropy of Composite MoS_2 Films. *Thin Solid Films* **1993**, *227*, 90–94.
34. Yu, Y.; Huang, S.-Y.; Li, Y.; Steinmann, S. N.; Yang, W.; Cao, L. Layer-Dependent Electrocatalysis of MoS_2 for Hydrogen Evolution. *Nano Lett.* **2014**, *14*, 553–558.
35. Lee, Y.-H.; Yu, L.; Wang, H.; Fang, W.; Ling, X.; Shi, Y.; Lin, C.-T.; Huang, J.-K.; Chang, M.-T.; Chang, C.-S.; *et al.* Synthesis and Transfer of Single-Layer Transition Metal Disulfides on Diverse Surfaces. *Nano Lett.* **2013**, *13*, 1852–1857.
36. Chiritescu, C.; Cahill, D. G.; Nguyen, N.; Johnson, D.; Bodapati, A.; Keblinski, P.; Zschack, P. Ultralow Thermal Conductivity in Disordered, Layered WSe_2 Crystals. *Science* **2007**, *315*, 351–353.
37. Böttner, H.; Venkatasubramanian, C. G. R. Aspects of Thin-Film Superlattice Thermoelectric Materials, Devices, and Applications. *Mater. Res. Soc. Bull.* **2006**, *31*, 211–217.